ISSN 1087-6596, Glass Physics and Chemistry, 2008, Vol. 34, No. 2, pp. 173–181. © Pleiades Publishing, Ltd., 2008.
Original Russian Text © A.E. Galashev, I.A. Izmodenov, 2008, published in Fizika i Khimiya Stekla.

# Computer Investigation of the Structure of $Si_{73}$ Clusters Surrounded by Hydrogen

**A. E. Galashev and I. A. Izmodenov**

*Institute of Industrial Ecology, Ural Division, Russian Academy of Sciences, ul. S. Kovalevskoi 20a, GSP-594, Yekaterinburg, 620219 Russia*

*e-mail: galashev@ecko.uran.ru*

Received June 8, 2007

**Abstract**—The stabilization of the structure of $Si_{73}$ clusters that are surrounded by 60 hydrogen atoms and subjected to seventeenfold stepwise heating from 35 to 1560 K (in steps of ~90 K) is investigated using the molecular dynamics method. The analysis is performed for clusters of three types, i.e., a particle assembled from an icosahedron and a fullerene, a nanocrystal, and a particle with a random atomic packing. In all cases, an increase in the temperature in the course of heating is accompanied by evaporation of a Si atom from the clusters and an increase in the size of silicon particles. The temperature of detachment of Si atoms from clusters is lowest for the cluster with a random atomic packing and highest for the nanocrystal. The nanoassembled particle has the most stable number (close to four) of Si–Si bonds per atom over the entire temperature range $35 \le T \le 1560$ K. For each type of $Si_{73}$ clusters, the mean length of the Si–Si bond decreases with an increase in the temperature. According to the radial distribution functions, the $Si_{73}$ clusters have different structures even at the temperature $T = 1560$ K. The distributions of bond angles reflect the presence of fourfold symmetry elements in the nanoassembled cluster and the nanocrystal. The relative depth of "penetration" of hydrogen atoms into the cluster is largest for the nanocrystal and smallest for the nanoassembled nanoparticle. The largest number of hydrogen atoms is "adsorbed" on the particle with a random atomic packing.

**DOI:** 10.1134/S1087659608020107

## INTRODUCTION

The particular interest expressed by researchers in silicon nanoparticles is associated primarily with the use of these objects in optoelectronics. Owing to the small sizes of these nanoparticles, their electronic properties are substantially affected by the quantum effects. Nanomaterials should satisfy stringent requirements for the size of particles, their shape, and purity. A high concentration of small-sized particles can be achieved in the course of gas condensation. However, the preparation of an ultradispersed fraction is complicated by a fast coagulation. The final size of primary spherical particles and their agglomeration are determined by the ratio of the time between particle collisions to the coalescence time. The coalescence is observed when the characteristic time of this process is longer than the characteristic time between particle collisions. In principle, by varying these times, it is possible to control the morphology and size of particles. There are two ways for controlling the primary size of particles: a change in the characteristic time between collisions through dilution (i.e., a decrease in the particle concentration in the flow) and a change in the coalescence time.

However, there exists one more approach providing a decrease in the reactivity of collisions. The surface of silicon nanoparticles ($N > 200$) can be passivated by hydrogen in the temperature range 300–1800 K [1]. When hydrogen is present at the surface of nanoparticles, they bounce off each other even in the liquid state. According to the model concept of the diffusion in the solid state, the characteristic coalescence time can be written in the form [2–4]

$$\tau_f = \frac{3nkT_p}{64\pi\sigma D}, \quad (1)$$

where $T_p$ is the particle temperature, $n$ is the particle number concentration, $D$ is the diffusion coefficient in the solid state, $\sigma$ is the surface tension of a particle, and $k$ is the Boltzmann constant.

In the case of a viscous flow, the coalescence time is defined by the relationship [5]

$$\tau_f = \frac{\eta d_p}{\sigma}, \quad (2)$$

where $d_p$ is the particle diameter and $\eta$ is the viscosity dependent on the temperature. The melting temperature is equal to 1683 K for crystalline silicon and 1210 K for crystalline germanium. As a rule, expression (1) is used for estimating the coalescence time for silicon nanoparticles in the solid state in the temperature range ($1213 \le T \le 1273$ K) of preparation of nanoparticles from this semiconductor. Relationship (2) serves for the determination of the coalescence time for germanium nanoparticles.

The growth of aerosol particles in the regime of suppression of the coalescence corresponds to the conditions where the coalescence time is inversely proportional to the particle growth rate. Without going into a detailed model of particle growth, we can make the inference that the shape and size of experimentally grown nanoparticles are related to the temperature through the change in the coalescence time. The surface properties have a significant effect on the coalescence time $\tau_f$. In actual fact, the coalescence is governed by the minimization of the surface free energy. The passivation of the surface by hydrogen considerably decreases the surface tension of silicon nanoparticles with sizes from 2 to 10 nm and only insignificantly increases the self-diffusion coefficient of Si atoms [6]. The electronic and optical properties of hydrogenated amorphous silicon are considered in [7–9].

Spatially controlled nanocomposites with high functional capabilities have already been synthesized to date [10]. Fuel cells in the form of electrolytic membranes based on silicon with the use of gas (hydrogen) and liquid (methanol) fuels have been tested [11], and miniature gas chromatographs capable of separating and identifying complex gas mixtures in a few seconds have been designed [12]. Small-sized semiconductor nanostructures and organic molecules have opened up unique possibilities based on an extremely low dissipated power, quantum effects, and surface sensitivity.

The $Si_{60}$ cluster in the ground state has a nonzero spin and, hence, belongs to materials with a molecular magnetism [13]. Unlike valently unsaturated, i.e., open, structures (such as $Si_{60}$), "closed structures" of the $Si_{60}H_{60}$ type are nonmagnetic.

The purpose of the present work was to investigate how the temperature affects the bulk and surface structures of three 73-atom silicon nanoparticles surrounded by 60 hydrogen atoms. The silicon nanoparticles are fragments of a diamond-like lattice or a random atomic packing, as well as a nanoassembly formed by a 60-atom fullerene containing a 13-atom icosahedron.

## THE TERSOFF POTENTIAL

Tersoff [14, 15] proposed a new form of binding of two atoms in a model with due regard for many-atom correlations. The main idea is that, in real systems, the strength of each bond depends on the local environment, so that bonds formed by an atom with many neighbors are weaker than those formed with several nearest neighbors. The Tersoff potential can be represented in the following form [14, 15]:

$$U = \frac{1}{2}\sum_{i \neq j} V_{ij}, \quad V_{ij} = f_C(r_{ij})[f_R(r_{ij}) + b_{ij} f_A(r_{ij})], \quad (3)$$

where $r_{ij}$ is the distance between the $i$th and $j$th atoms; $f_A$ and $f_R$ are the attractive and repulsive pair potentials, respectively; and $f_C$ is the smooth cut-off function. The potentials $f_A$ and $f_R$ in an explicit form are represented by the Morse potentials

$$f_R(r) = Ae^{-\lambda_1 r}, \quad f_A(r) = -Be^{-\lambda_2 r}, \quad (4)$$

$$f_C(r) = \begin{cases} 1, & r < R - D \\ \frac{1}{2} - \frac{1}{2}\sin\left[\frac{\pi}{2}(r - R)/D\right], & R - D < r < R + D \\ 0, & r > R + D. \end{cases} \quad (5)$$

The parameters $A$ and $B$ determine the repulsive and attractive forces, respectively. The parameters $R$ and $D$ are chosen in such a way as to include only the layer of the first nearest neighbors in the bulk structures of silicon, graphite, and diamond. The smooth cut-off function $f_C$ decreases from 1 to 0 in the range $R - D < r < R + D$. The main feature of this potential is the presence of the term $b_{ij}$. The bonding force depends on the local environment and decreases when the number of neighbors is large. This behavior of the bonding is governed by the term $b_{ij}$, which increases or decreases the ratio between the attractive and repulsive forces according to the relationship

$$b_{ij} = \frac{1}{(1 + \beta^n \zeta_{ij}^n)^{1/2n}}, \quad (6)$$

where

$$\zeta_{ij} = \sum_{k \neq i, j} f_C(r_{ij}) g(\theta_{ijk}) e^{[\lambda_3^3 (r_{ij} - r_{ik})^3]},$$
$$g(\theta) = 1 + \frac{c^2}{d^2} - \frac{c^2}{[d^2 + (h - \cos\theta)^2]}. \quad (7)$$

The term $\zeta_{ij}$ characterizes the effective coordination number of the $i$th atom, i.e., the number of the nearest neighbors. This number is determined with allowance made for the relative distance between two neighbors $r_{ij} - r_{ik}$ and the bond angle $\theta$. The function $g(\theta)$ describes the dependence of the coordination number on the bond angle. The parameter $d$ characterizes the rate of change of the function $g(\theta)$. The parameter $c$ specifies the dependence of the force on the angle $\theta$. The parameters of the potential $V_{ij}$ were chosen by fitting the theoretical and experimental data obtained for real and hypothetical configurations. These data involved the bonding energy, the lattice constant, and the bulk modulus. The parameters of the Tersoff potential used for silicon are presented in Table 1. In the initial packing composed of the fullerene with the inscribed extended icosahedron, there are five fullerene atoms located at the distance equal to the bond length $L_b = 0.24$ nm for each atom positioned on the icosaherdron surface. For an atom of the icosahedron surface, the five nearest neighbors also

**Table 1.** Parameters of the Tersoff potential for silicon

| $A$ | $B$ | $\lambda_1$ | $\lambda_2$ | $\lambda_3$ | $n$ | $c$ | $d$ | $R$ | $D$ | $\beta$ | $h$ |
|---|---|---|---|---|---|---|---|---|---|---|---|
| eV | | $nm^{-1}$ | | | | | | nm | | | |
| 1830.0 | 471.18 | 2.4799 | 1.7322 | 0 | 0.78734 | $1.0039 \times 10^5$ | 16.217 | 0.285 | 0.015 | $1.1 \times 10^{-6}$ | –0.59825 |

**Table 2.** Parameters of the potentials of the Si–H and H–H interactions

| $A_1$ | $A_2$ | $\lambda_1$ | $\lambda_2$ | $B_H$, eV | $\alpha$ | $\alpha_H$ | $r_{c_1}$ | $r_{c_2}$ | $\mu_1$ | $\mu_2$ | $\varepsilon$, eV | $\alpha_{HH}$ | $r_m$, nm |
|---|---|---|---|---|---|---|---|---|---|---|---|---|---|
| eV | | $nm^{-1}$ | | | $nm^{-2}$ | | nm | | | | | | |
| 1113.967 | –700 | 27.801 | 23.616 | 22.6526 | 30.34373 | 60.334 | 0.39527357 | 0.18 | 0.0312058 | 0.02 | 0.147 | 15.20 | 0.19 |

lying on the icosahedron surface can be disregarded, because the distance to these atoms is ~1.9 times larger than the bond length $L_b$ and the distance from the icosahedron center to atoms on its surface is 1.8 times larger than the bond length $L_b$. The attraction of the fullerene by the icosahedron is provided by 60 bonds.

## REPRESENTATION OF THE Si–H AND H–H INTERACTIONS

When simulating the Si–H interactions, there arises a problem of control of the univalence of hydrogen. Mousseau and Lewis [16] simulated an amorphous Si–H system with the use of the approach based on different potentials describing the bonded and nonbonded S–H interactions. The molecular dynamics calculations within this approach appear to be very slow virtually at any finite temperature. Kwon et al. [17] proposed the potential that describes the Si–H interactions in an arbitrary configuration without necessity of including bonded and nonbonded Si–H pairs. This potential consists of two parts, one of which describes the pair interactions and the other part represents the triple interactions. The Si–H two-particle potential is written in the form

$$V^{(2)}_{\text{Si–H}} = [A_1 \exp(-\lambda_1 r) + A_2 \exp(-\lambda_2 r)] f^{\text{H}}_c(r), \quad (8)$$

where $f^{\text{H}}_c$ is the cut-off function given by the formula

$$f^{\text{H}}_c(r) = \begin{cases} 1, & r \le 0.17 \text{ nm} \\ 0.5 + 0.5\cos[(\pi/0.2)(r - 0.17)], & 0.17 < r < 0.19 \text{ nm} \\ 0, & r \ge 0.19 \text{ nm}. \end{cases} \quad (9)$$

The parameters $A_1$, $A_2$, $\lambda_1$, and $\lambda_2$ obtained by fitting to the ab initio calculated energy of hydrogen on a silicon cluster [17] are listed in Table 2. The two-particle potential described by formulas (8) and (9) leads to a minimum energy of –3.05 eV at $r = 0.15$ nm, which is in good agreement with the energy of the Si–H bond and the mean bond length in the Si–H amorphous system. This potential also results in a frequency of 2023 $cm^{-1}$ for the stretching vibration mode of the Si–H bond, which also agrees well with the experimental frequency of this mode. The short-range character of the interaction is provided by the cut-off function $f^{\text{H}}_c$, which can be represented in the form of a simple smooth functional.

The three-particle potential, which is important for simulating the Si–H covalent interaction and stabilizing the tetrahedral structure of silicon, is written in the form [18]

$$V^{(3)}(r_{12}, r_{13}, \theta) = B_{\text{H}} \varphi_{1,2}(r_{12}) \varphi_2(r_{13}) \times (\cos\theta + 1/3)^2 g_{c_{1,2}}(r_{12}) g_{c_2}(r_{13}). \quad (10)$$

The indices 1 and 2 correspond to the Si–Si and Si–H interactions, respectively. The radial functions $\varphi_1(r)$ and $\varphi_2(r)$ are defined as $\varphi_1(r) = \exp(-\alpha r^2)$ and $\varphi_2(r) = \exp(-\alpha_{\text{H}} r^2)$. The cut-off functions ($g_{c_1}$, $g_{c_2}$) are represented in the form $g_{c_{1,2}}(r) = \{1 + \exp[(r - r_{c_{1,2}})/\mu_{1,2}]\}^{-1}$. The parameters $B_{\text{H}}$, $\alpha$, $\alpha_{\text{H}}$, $r_{c_i}$, and $\mu_i$ are given in Table 2. The parameters $B_{\text{H}}$ and $\alpha_{\text{H}}$ were obtained by fitting of the rocking mode (630 $cm^{-1}$) and bending mode (897 $cm^{-1}$) for H–Si bond in amorphous Si:H. This potential describes the Si–Si–H, H–Si–H, and Si–H–Si interactions. It should be noted that the lowest energy is achieved when the H atom is bound to one Si atom.

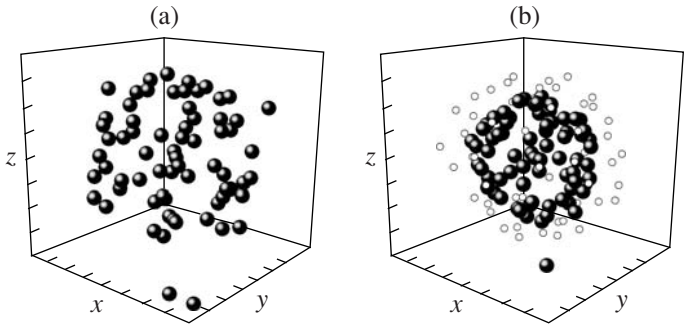


**Fig. 1.** Configurations of the $Si_{73}$ cluster composed of a 13-atom icosahedron and a 60-atom fullerene: (a) cluster with a free surface and (b) cluster surrounded by 60 hydrogen atoms at the instant of time $t$ = 100 ps and the temperature $T$ = 1560 K.

The used H–H repulsive potential in the form

$$V_{HH}^{(2)}(r) = [\varepsilon/(1-6/\alpha_{HH})] \times [(6/\alpha_{HH})\exp[\alpha_{HH}(1-r/r_m)] - (r/r_m)^6] \quad (11)$$

prevents nonphysical approach of hydrogen atoms to one another [17]. In this scheme, the formation of $H_2$ molecules is impossible. Only atomic hydrogen is included in the model. The parameters $\varepsilon$, $\alpha_{HH}$, and $r_m$ are presented in Table 2.

## THE MOLECULAR DYNAMICS MODEL OF $Si_{73}$ NANOPARTICLES

The molecular dynamics calculations were based on the integration of the equations of motion with the use of the fourth-order Runge–Kutta method. The time step $\Delta t$ was equal to $10^{-16}$ s. Three series of calculations were performed for silicon nanoparticles. The temperature of the initial state for each series of calculations was taken equal to 35 K. The duration of the calculations at each temperature was equal to 1000000 time steps or 100 ps. The final atomic configuration obtained at a lower temperature served as the initial configuration for the subsequent calculations at a higher temperature. In the calculations, the temperature was increased in steps of approximately 90 K. The last calculations were carried out at a temperature of 1560 K. In the first series of calculations, the initial configuration of the nanoparticle was represented by the nanoassembly composed of a 60-atom fullerene into which a 13-atom icosahedron was inserted. The minimum distance (0.24 nm) between the atoms in this nanoassembly was close to the minimum distance between atoms in the silicon macrocrystal (0.235 nm). In the second series of calculations, a fragment composed of a particular site with 72 nearest neighbors in the diamond lattice was used as the initial configuration. In the initial state, the density of the crystalline nanoparticle corresponded to that of the macrocrystalline material. In the third series of calculations, a fragment with a random atomic packing served as the initial configuration. This configuration of the nanoparticle was produced by filling a spherical region of the corresponding radius with silicon atoms by using a random-number generator. In the initial state, the minimum distance between silicon atoms in the random packing did not exceed the minimum distance in the corresponding macrocrystal. As a result (and also in view of a decrease in the time of filling the sphere), the initial nanoparticle had a looser atomic packing. The nanoparticle density was no higher than 0.6 of the density of the silicon nanocrystal.

Each $Si_{73}$ particle was placed in a virtual sphere of the same diameter. The radius of the sphere was chosen so that 60 hydrogen atoms located at a distance of no less than 0.22 nm from each other can be randomly positioned in the space between the particle and the surface of the sphere. Therefore, the initial density of the hydrogen "coat" was approximately equal to 42–45 kg/m$^3$. It should be noted that the experimental density of liquid hydrogen at 20 K is approximately equal to 70 kg/m$^3$. The calculations for silicon particles surrounded by the hydrogen coat were performed using a canonical ensemble. The initial temperature (35 K) exceeded the boiling temperature of real hydrogen (20 K), so that the hydrogen environment of the nanoparticle even in the first calculation was a dense gas.

## THE INFLUENCE OF HYDROGEN ON THE STABILITY OF $Si_{73}$ CLUSTERS

The hydrogen coat has a clear stabilizing effect on the $Si_{73}$ nanoparticle but does not provide the retention of the structure at a high temperature and does not prevent the evaporation of Si atoms. Figure 1 depicts the configurations of the $Si_{73}$ nanoassembled clusters after a seventeenfold stepwise increase in the temperature, so that their kinetic energy approximately corresponds to a temperature of 1560 K. It can be seen from Fig. 1a that, in the absence of hydrogen, the $Si_{73}$ cluster has strongly expanded and lost five atoms by the instant of time 100 ps ($T$ = 1560 K), two of which are shown in the lower part of Fig. 1a. In the presence of the hydrogen coat (Fig. 1b), the silicon cluster composed of the fullerene and the icosahedron even at this high temperature retains a spherical shape and only one of its atoms evaporates (this atom is shown in the lower part of Fig. 1b). Although the silicon cluster surrounded by hydrogen is expanded, its expansion is less pronounced than that of the cluster in the absence of the hydrogen coat.

The internal energy of the $Si_{73}$ cluster in the form of the diamond lattice fragment surrounded by the hydrogen coat smoothly increases from –5.18 eV/atom at 35 K to –2.65 eV/atom at 1560 K (Fig. 2a). The other two $Si_{73}$ clusters surrounded by hydrogen have stronger temperature dependences of the internal energy. In this case, the internal energy $U$ for the nanoassembled clus-

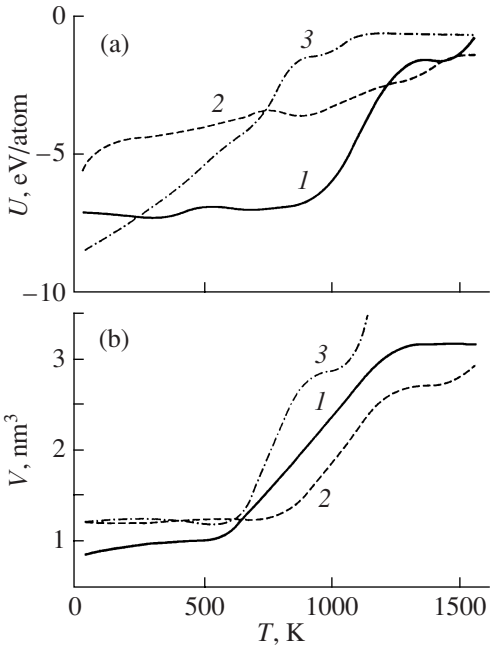


**Fig. 2.** Temperature dependences of (a) the internal energy of silicon clusters and (b) the volume of the virtual sphere bounding all atoms in the system: (*1*) nanoassembled particle, (*2*) nanocrystal, and (*3*) particle with a random atomic packing.

ter retains values comparable to those of crystalline silicon (–4.36 eV/atom) [19] up to a temperature of 1112 K (–4.33 eV/atom). The internal energy of the cluster with the random packing rapidly increases with an increase in the temperature, especially in the temperature range $690 \le T \le 850$ K. At $T = 750$ K, the internal energy of this cluster reaches the internal energy $U$ for the $Si_{73}$ nanocrystal. This behavior of the internal energy $U$ is associated with the considerable transformation of the cluster structure. The particle with the random atomic packing, the nanoassembled particle, and the nanocrystal each lose one Si atom at temperatures of 760, 850, and 1120 K, respectively. The internal energy $U$ at temperatures above these values was determined for $Si_{72}$ clusters.

The temperature dependences of the volume of the sphere that is constructed from the center of mass of the cluster and contains all 73 atoms (including evaporated atoms) are plotted in Fig. 2b. The volume of the bounding sphere for the nanoassembled cluster and the cluster with the random atomic packing is retained (accurate to within 20%) only to a temperature of ~600 K, whereas the volume of the sphere circumscribed around the nanocrystal is retained (accurate to within 3%) up to a temperature $T \approx 750$ K. The atom is completely detached from the cluster (the Si–Si bonds of this atom with the cluster disappear completely) at higher temperatures.

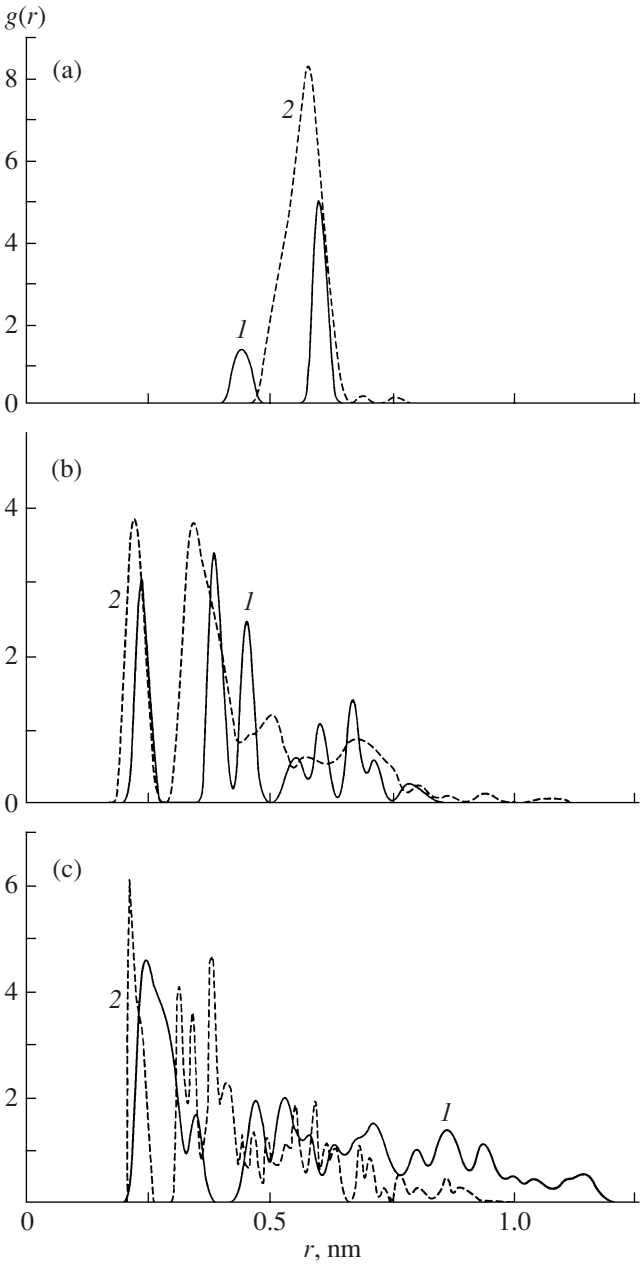


**Fig. 3.** Radial distribution functions for $Si_{73}$ clusters at temperatures of (*1*) 35 and (*2*) 1560 K: (a) nanoassembled particle, (b) nanocrystal, and (c) particle with a random atomic packing.

## STRUCTURE OF $Si_{73}$ CLUSTERS IN THE PRESENCE OF HYDROGEN ON THEIR SURFACE

The radial distribution function $g(r)$ was constructed for the atom located most closely to the center of mass of the cluster. This construction of the radial distribution function $g(r)$ for the clusters allows one to correctly take into account a spherical symmetry of the function. Figure 3 shows the calculated radial distribution functions for the $Si_{73}$ clusters at temperatures of 35 and 1560 K. The radial distribution function for the

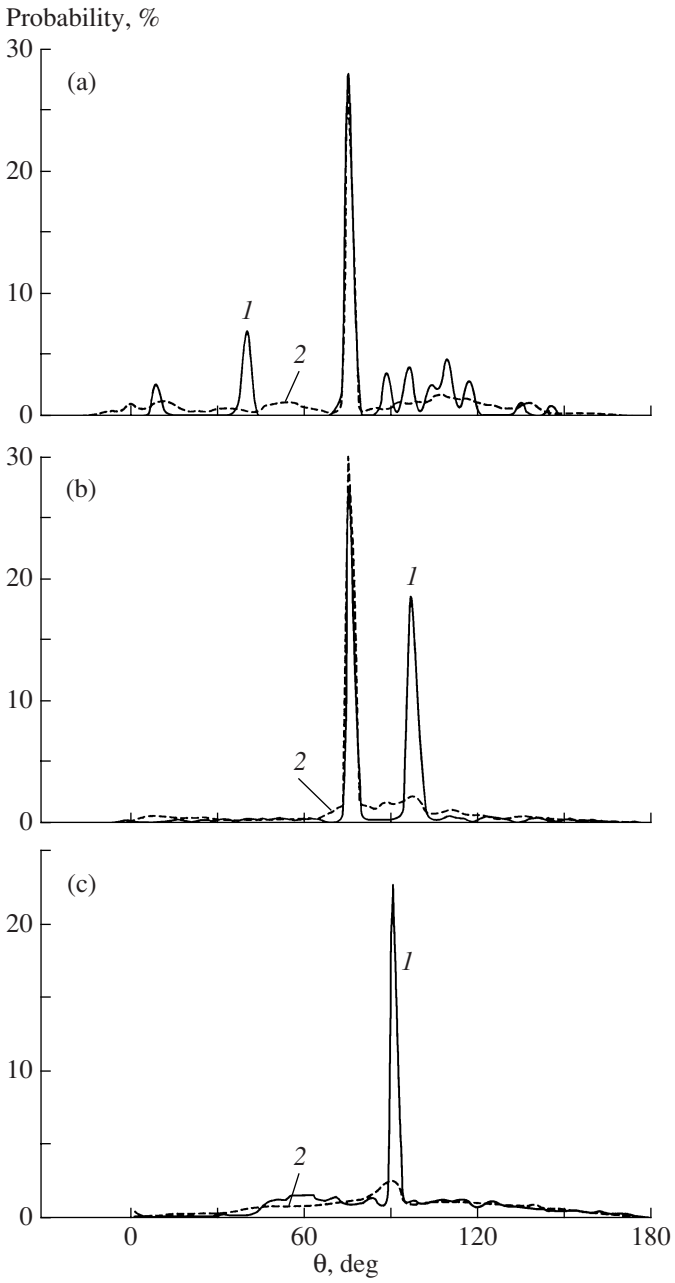


**Fig. 4.** Distributions of bond angles θ in $Si_{73}$ clusters at temperatures of (*1*) 35 and (*2*) 1560 K. The letter designations are the same as in Fig. 3.

nanoassembled cluster at $T = 35$ K exhibits two well-resolved peaks. The first (low-intensity) peak is governed by the twelve nearest neighbors located at the surface of the icosahedron. The second (high-intensity) peak is determined by the 60 next nearest neighbors corresponding to the fullerene. At $T = 1560$ K, there is only one peak (broader and with a higher intensity), the maximum of which is shifted toward smaller distances by $\Delta r = 0.022$ nm with respect to the position of the second peak of the radial distribution function $g(r)$ at 35 K. The radial distribution function of the $Si_{73}$ nanocrystal has eight peaks at a temperature of 35 K and only four peaks at $T = 1560$ K (except for oscillations in its tail portion). The first and second peaks of the radial distribution function $g(r)$ are shifted toward smaller distances by $\Delta r = 0.022$ and 0.043 nm, respectively. The third peak of the radial distribution function is shifted toward larger distances by $\Delta r = 0.044$ nm. The fourth broad peak at $r_{\max_4} = 0.673$ nm replaces the other five peaks of the radial distribution function $g(r)$ for the nanocrystal at a temperature of 35 K. The radial distribution function for the cluster with the random atomic packing at $T = 35$ K has a large number of predominantly poorly resolved peaks. The tail of this function extends to ~1.20 nm, and the first peak of the radial distribution function $g(r)$ is located at 0.239 nm. After heating to a temperature of 1560 K, the tail of the radial distribution function $g(r)$ extends to only ~0.925 nm and the first peak is located at $r_{\max_1} = 0.215$ nm.

The distributions of the angles θ formed by the Si–Si bonds in the $Si_{73}$ clusters at temperatures of 35 and 1560 K are shown in Fig. 4. In all the cases under consideration, the angle $\theta = 91.8°$ is dominant. For the nanoassembled cluster at $T = 1560$ K, the height of the first peak at 91.8° decreases by 4.6% and all the other peaks (at angles differing from 91.8°) are smeared. Upon heating of the $Si_{73}$ nanocrystal from 35 to 1560 K, the peak at 110° completely disappears in the distribution of the angles θ and the intensity of the peak at 91.8° increases by 11.4%. In the distribution of the angles θ for the cluster with the random atomic packing, the intensity of the peak at 91.8° decreases almost ten times with an increase in the temperature by 1525 K.

The Si–Si covalent bond is a short-range bond. The cut-off function $f_C(r)$ defined by expression (5) cuts off the Si–Si pair interactions at distances exceeding 0.3 nm. Let us assume that the criterion for the existence of the Si–Si bond is represented by the condition $r_{\text{Si–Si}} < 0.3$ nm. By using this criterion for the determination of distances $r_{\text{Si–Si}}$ between the current Si atom and all the other Si atoms in the cluster, it is possible to calculate the mean number $\bar{n}_b$ of bonds per atom and the mean length $\bar{L}_b$ of the Si–Si bonds. The calculated values of $\bar{n}_b$ and $\bar{L}_b$ for the $Si_{73}$ clusters in the temperature range $35 \le T \le 1560$ K are presented in Fig. 5. At low temperatures ($T < 630$ K), the values of $\bar{n}_b$ and $\bar{L}_b$ for the nanoparticle with the random atomic packing are larger than those for the other clusters under consideration. These parameters for all the clusters under investigation decrease with an increase in the temperature. Upon heating by 1525 K, the mean number $\bar{n}_b$ of bonds in the cluster with the random atomic packing decreases most drastically (by approximately 30%). The mean numbers $\bar{n}_b$ of bonds in the nanoassembled

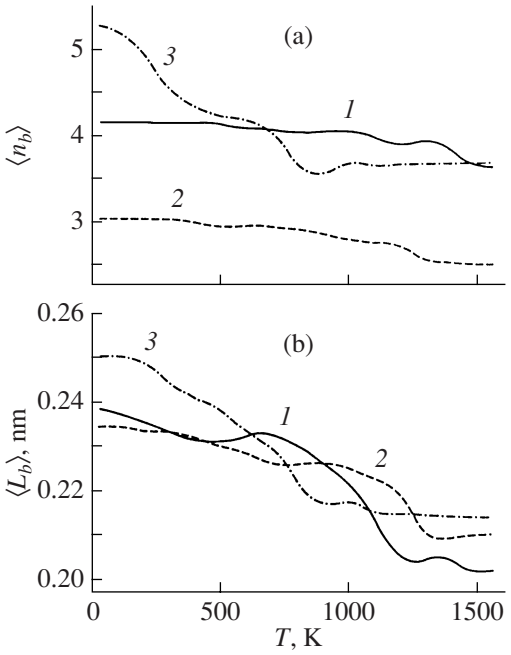


**Fig. 5.** Temperature dependences of (a) the mean number of Si–Si bonds per atom in $Si_{73}$ clusters and (b) the mean length of these bonds. The number designations are the same as in Fig. 2.

cluster and the nanocrystal decrease by 12 and 17%, respectively. It should be noted that, at temperatures above 690 K, the values of $\bar{n}_b$ for the nanoassembled particle, as a rule, are larger than those for the other particles under investigation. The nanocrystal has the smallest values of $\bar{n}_b$ over the entire temperature range.

At a temperature of 35 K, the mean bond length $\bar{L}_b$ for the particles with noncrystalline packings is larger than the mean bond $\bar{L}_b^{\text{cryst}}$ for the silicon crystal (0.235 nm). The equality $\bar{L}_b = \bar{L}_b^{\text{cryst}}$ is observed at $T =$ 250 K for the nanoassembled particle and $T = 592$ K for the particle with the random atomic packing. Upon heating to 1560 K, the mean bond lengths $\bar{L}_b$ for the nanoassembled nanoparticle, the nanocrystal, and the particle with the random atomic packing decrease by 15, 10, and 14%, respectively. The mean bond lengths $\bar{L}_b$ for the particle formed by inserting the icosahedron into the fullerene and the particle with the random atomic packing decrease most rapidly in the ranges $710 \le T \le 1230$ K and $170 \le T \le 890$ K, respectively. As a result, the smallest mean bond lengths $\bar{L}_b$ at $T >$ 1090 K are observed for the particle composed of the fullerene and the icosahedron. At $T > 1260$ K, the mean bond lengths $\bar{L}_b$ for the nanocrystal again become smaller than those of the particle with the random atomic packing.

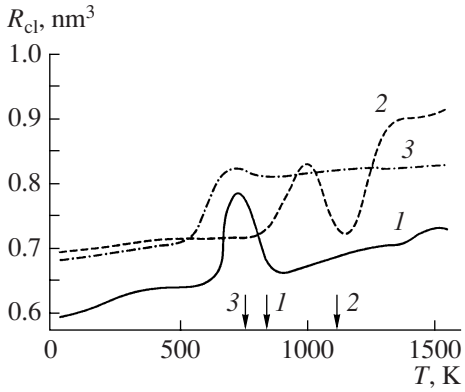


**Fig. 6.** Temperature dependences of the radius of silicon clusters. The number designations are the same as in Fig. 2. Arrows indicate the temperatures of the onset of evaporation of Si atoms from clusters.

## THE SURFACE RELIEF OF THE $Si_{73}$ CLUSTERS AND HYDROGEN ADSORPTION

The cluster radius $R_{cl}$ is defined as the length of the segment from the center of mass of the cluster to the center of the Si atom that belongs to the cluster and is most distant from the center of mass. The temperature dependences of the radius $R_{cl}$ for the particles under consideration are plotted in Fig. 6. The dependences $R_{cl}(T)$ for the particles reflect the evaporation of atoms from the solid cluster. The peak in the dependence $R_{cl}(T)$ for the $Si_{73}$ cluster with the random atomic packing is observed at the lowest temperature. This peak indicates that the atom evaporates from the particle. A similar peak for the nanoassembled cluster appears at a higher temperature. The corresponding peak in the dependence $R_{cl}(T)$ for the nanocrystal occurs at the highest temperature. The arrows near the abscissa axis indicate the temperatures of the onset of evaporation. The evaporation begins at a somewhat higher temperature $T$ than the temperature at which the peak is located in the corresponding dependence $R_{cl}(T)$ due to the discreteness of the change in the temperature. The detachment of the atom from the cluster leads to a decrease in the cluster radius $R_{cl}$, because the number of atoms contained in the cluster becomes smaller by unity. At a temperature of 1560 K, the nanoassembled cluster has the smallest size and the largest radius $R_{cl}$ is observed for the nanocrystal.

The degree of penetration of hydrogen atoms into the cluster can be defined as the ratio $\xi = (R_{cl} - R_H)/R_{cl}$, where $R_H$ is the distance from the center of mass of the silicon cluster to the hydrogen atom nearest to the center of mass. The temperature dependence $\xi(T)$ for the nanoassembled cluster exhibits a maximum at 746 K, and the degree of penetration $\xi$ beginning with 1100 K increases progressively (Fig. 7a). Two peaks are observed in the temperature range $0 \le T \le 1150$ K in the dependence $\xi(T)$ for the nanocrystal. The highest peak

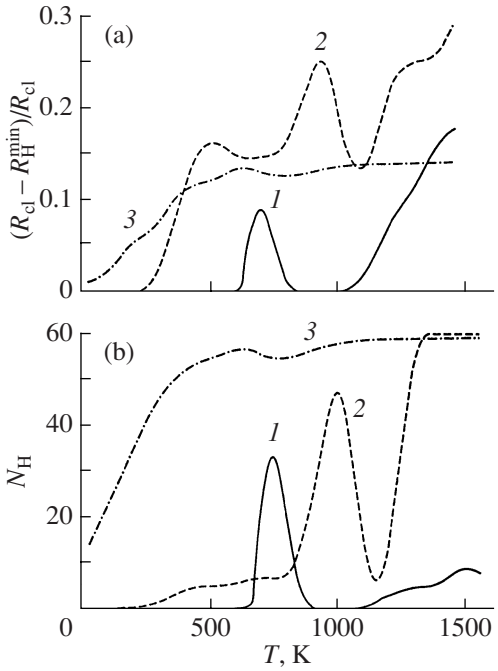


**Fig. 7.** Temperature dependences of (a) the relative depth of penetration of hydrogen atoms into the $Si_{73}$ clusters and (b) the number of hydrogen atoms adsorbed on these particles. The number designations are the same as in Fig. 2.

is located at a temperature of 1004 K. An increase in the temperature to 1165 K is accompanied by a monotonic increase in the quantity $\xi$ for the nanocrystal. The temperature dependence $\xi(T)$ for the cluster with the random atomic packing is rather smooth. However, this dependence also exhibits a small maximum at $T$ = 690 K. The locations of all the maxima at the above temperatures coincide with those in the corresponding dependences $R_{cl}(T)$.

The temperature dependences of the number $N_H$ of hydrogen atoms located in the spherical layer of thickness $(R_{cl} - R_H)$ for the clusters are depicted in Fig. 7b. Among the clusters under investigation, the $Si_{73}$ nanoassembled cluster has the smallest value of $N_H$. The maximum number $N_H = 33$ is observed at a temperature of 746 K immediately before the evaporation temperature. After subsequent heating of the cluster by ~90 K, the number $N_H$ becomes equal to zero. At temperatures above 1090 K, this quantity insignificantly increases to $N_H = 9$. The dependence of the number $N_H$ for the nanocrystal exhibits a maximum at $T$ = 1004 K ($N_H$ = 47). However, already after the next heating stage, the number $N_H$ decreases to 6. At a temperature of 1350 K, the number $N_H$ becomes equal to 60; i.e., all the H atoms are located in the surface nanocrystal layer of thickness $(R_{cl} - R_H)$. The dependence $N_H(T)$ for the cluster with the random atomic packing is characterized by a considerably smoother behavior. In this dependence, there is a small maximum ($N_H$ = 55) at the temperature $T$ = 690 K. The next extremum (minimum) turns out to be not deep ($N_H$ = 52), and the quantity $N_H$ at the temperature $T$ =1000 K reaches an almost maximum value ($N_H$ = 59).

## CONCLUSIONS

Thus, the results of the computer experiment demonstrated that the $Si_{73}$ clusters well adsorb hydrogen at low temperatures. The hydrogen coat is retained around these particles up to high temperatures (~1500–1600 K). The hydrogen atoms are repelled from each other and, thus, have a compressive effect on the cluster. The coat stabilizes the nanoparticles at temperatures below 600 K. However, at higher temperatures, Si atoms can evaporate from the clusters. The nanoparticle composed of the icosahedron and the fullerene retains the highest density up to a temperature of 1560 K. Two concentric atomic layers of this nanoparticle are mixed at high temperatures. As a consequence, the corresponding radial distribution function exhibits one peak instead of two peaks.

The crystal lattice of diamond has a tetrahedral ordering. As the temperature increases, the ordering of the $Si_{73}$ clusters under investigation becomes nontetrahedral. At a temperature of 1560 K, the tetrahedral angle of 109.5° appears to be weakly pronounced in the distribution of the bond angles $\theta$ and manifests itself as a small peak only for the nanoassembled particle. The peak at 109.5° in the distribution of the bond angles $\theta$ for the other two particles virtually disappears. In the high-temperature range, the angle of 91.8° is dominant in the distributions of the bond angles $\theta$ for the nanoassembled particle and the nanocrystal. This means that the structure of each particle under consideration is characterized by a fourfold symmetry element. The nanoassembled particle has the most stable number (close to four) of Si–Si bonds per atom in the temperature range $35 \le T \le 1560$ K. In each particle under investigation, the mean bond length decreases and the particle size $R_{cl}$ increases with an increase in the temperature. Moreover, the particle shape does not deviate significantly from a spherical shape. As a result, holes should be formed inside the particles, and these holes can be occupied by hydrogen. The practical importance of our investigation is associated with the use of hydrogen as a fuel.

## REFERENCES

1. Hawa, T. and Zachariah, M.R., Molecular Dynamics Study of Particle–Particle Collisions between Hydrogen-Passivated Silicon Nanoparticles, *Phys. Rev. B: Condens. Matter*, 2004, vol. 69, p. 035417 (1–9).
2. Ehrman, S.H., Friedlander, S.K., and Zachariah, M.R., Characteristics of $SiO_2/TiO_2$ Nanocomposite Particles Formed in a Premixed Flat Flame, *J. Aerosol Sci.*, 1998, vol. 29, nos. 5–6, pp. 687–706.

3. Windeler, R.S., Lehtinen, K.E.J., and Friedlander, S.K., Production of Nanometer-Sized Metal Oxide Particles by Gas Phase Reaction in a Free Jet. I: Experimental System and Results, *Aerosol Sci. Technol.*, 1997, vol. 27, no. 2, pp. 174–190.
4. Biswas, P., Yang, G., and Zachariah, M.R., In Situ Processing of Ferroelectric Materials from Lead Waste Streams by Injection of Gas Phase Titanium Precursors: Laser Induced Fluorescence and X-ray Diffraction Measurements, *Combust. Sci. Technol.,* 1998, vol. 134, nos. 1–6, pp. 183–200.
5. Frenkel, Ya.I., *Kineticheskaya teoriya zhidkostei* (Kinetic Theory of Liquids), Leningrad: Nauka, 1975 [in Russian].
6. Hawa, T. and Zachariah, M.R., Internal Pressure and Surface Tension of Bare and Hydrogen Coated Silicon Nanoparticles, *J. Chem. Phys.*, 2004, vol. 121, no. 18, pp. 9043–9049.
7. Zhang, R.Q., Costa, J., and Bertran, E., Role of Structural Saturation and Geometry in the Luminescence of Silicon-Based Nanostructured Materials, *Phys. Rev. B: Condens. Matter*, 1996, vol. 53, no. 12, pp. 7847–7850.
8. Delley, B. and Steigmeier, E.F., Size Dependence of Band Gaps in Silicon Nanostructures, *Appl. Phys. Lett.*, 1995, vol. 67, no. 16, pp. 2370–2372.
9. Filonov, A.B., Kholod, A.N., Borisenko, V.E., et al., Oxygen Effect on Optical Properties of Nanosize Silicon Clusters, *Phys. Rev. B: Condens. Matter*, 1998, vol. 57, no. 3, pp. 1394–1397.
10. Yu, B. and Meyyappan, M., Nanotechnology: Role in Emerging Nanoelectronics, *Solid-State Electron.*, 2006, vol. 50, pp. 536–544.
11. Xiao, Zh., et al., A Silicon-Based Fuel Cell Micro Power System Using a Microfabrication Technique, *J. Micromech. Eng.*, 2006, vol. 10, no. 16, pp. 2014–2020.
12. Wise, K.D., Integrated Sensors, MEMS, and Microsystems: Reflection on a Fantastic Voyage, *Sens. Actuators, A*, 2007, vol. 136, pp. 39–50.
13. Polukhin, V.A., *Modelirovanie nanostruktury i prekursornykh sostoyanii* (Simulation of Nanostructures and Precursor States), Yekaterinburg: Ural. Otd. Ross. Akad. Nauk, 2004.
14. Tersoff, J., New Empirical Approach for the Structural and Energy of Covalent Systems, *Phys. Rev. B: Condens. Matter*, 1988, vol. 37, no. 10, pp. 6991–7000.
15. Tersoff, J., Modeling Solid-State Chemistry: Interatomic Potentials for Multicomponent Systems, *Phys. Rev. B: Condens. Matter*, 1989, vol. 39, no. 8, pp. 5566–5568.
16. Mousseau, N. and Lewis, L.J., Dynamical Models of Hydrogenated Amorphous Silicon, *Phys. Rev. B: Condens. Matter*, 1991, vol. 43, pp. 9810–9817.
17. Kwon, I., Biswas, R., and Soukoulis, C.M., Molecular-Dynamics Simulations of Defect Formation in Hydrogenated Amorphous Silicon, *Phys. Rev. B: Condens. Matter*, 1992, vol. 45, no. 7, pp. 3332–3339.
18. Biswas, P. and Hamman, D.R., New Classical Models for Silicon Structural Energies, *Phys. Rev. B: Condens. Matter*, 1987, vol. 36, no. 12, pp. 6434–6445.
19. Yin, M.T. and Cohen, M.L., Theory of Static Structural Properties, Crystal Stability, and Phase Transformations: Application to Si and Ge, *Phys. Rev. B: Condens. Matter*, 1982, vol. 26, no. 10, pp. 5668–5687.